

pubs.acs.org/JPCA Article

Capturing CO₂ in Quadrupolar Binding Pockets: Broadband Microwave Spectroscopy of Pyrimidine- $(CO_2)_n$, n = 1,2

Blair A. Welsh, Andres S. Urbina, Tuan A. Ho, Susan L. Rempe, Lyudmila V. Slipchenko,* and Timothy S. Zwier*



Cite This: J. Phys. Chem. A 2024, 128, 1124–1133



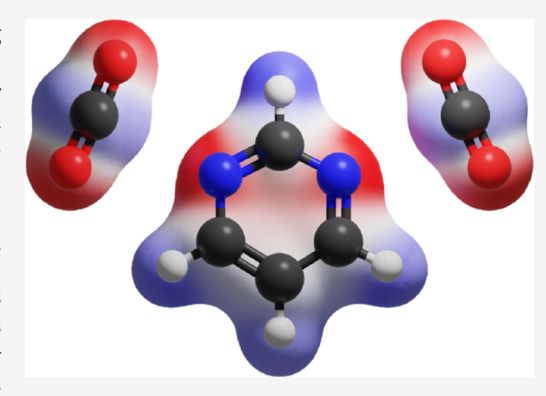
ACCESS I

Metrics & More

Article Recommendations

Supporting Information

ABSTRACT: Pyrimidine has two in-plane $CH(\delta+)/N(\delta-)/CH(\delta+)$ binding sites that are complementary to the $(\delta - /2\delta + /\delta -)$ quadrupole moment of CO₂. We recorded broadband microwave spectra over the 7.5-17.5 GHz range for pyrimidine- $(CO_2)_n$ with n = 1 and 2 formed in a supersonic expansion. Based on fits of the rotational transitions, including nuclear hyperfine splitting due to the two ¹⁴N nuclei, we have assigned 313 hyperfine components across 105 rotational transitions for the n = 1 complex and 208 hyperfine components across 105 rotational transitions for the n = 2 complex. The pyrimidine-CO₂ complex is planar, with CO2 occupying one of the quadrupolar binding sites, forming a structure in which the CO₂ is stabilized in the plane by interactions with the C-H hydrogens adjacent to the nitrogen atom. This structure is closely analogous to that of the pyridine-CO₂ complex studied previously by (Doran, J. L.et al. J. Mol. Struct. **2012**, 1019, 191–195). The fit to the n=2



cluster gives rotational constants consistent with a planar cluster of $C_{2\nu}$ symmetry in which the second CO_2 molecule binds in the second quadrupolar binding pocket on the opposite side of the ring. The calculated total binding energy in pyrimidine- CO_2 is -13.7kJ mol⁻¹, including corrections for basis set superposition error and zero-point energy, at the CCSD(T)/ 6-311++G(3df,2p) level, while that in pyrimidine-(CO₂)₂ is almost exactly double that size, indicating little interaction between the two CO₂ molecules in the two binding sites. The enthalpy, entropy, and free energy of binding are also calculated at 300 K within the harmonic oscillator/rigidrotor model. This model is shown to lack quantitative accuracy when it is applied to the formation of weakly bound complexes.

I. INTRODUCTION

The accelerating pace of global climate change and its potentially catastrophic outcomes have created an urgent need for mitigation strategies for reducing CO2 in our atmosphere. One of the most obvious strategies to consider is also the most difficult; namely, to directly extract CO2 from ambient air.²⁻⁴ The challenge is considerable, as CO₂ is present at <500 ppm in the atmosphere, yet it needs to be removed selectively relative to the major components of air (N_2, O_2) , which are present at concentrations 1600 and 400 times greater, respectively, at 25 °C. High selectivity can be achieved through the chemical reaction of CO2, typically by forming carbamate (R₂-NH⁺-CO₂⁻), bicarbonate (HCO₃⁻), or carbonate (CO₃²⁻) anions.⁵ However, significant energy must be expended to regenerate captured materials, increasing the cost of the process.

Physisorption of CO2 greatly reduces the energetic cost of regenerating captured materials. However, there is a steep entropic cost that accompanies complex formation, which puts a bound on the required strength of binding of $\Delta H \leq -30 \text{ kJ}$ mol^{-1} .

The move from chemisorption to physisorption also brings with it the challenge of achieving strong selectivity of CO₂ binding over N2 and O2, as all three molecules are nonpolar linear molecules that might be anticipated to interact similarly toward physisorption binding partners. In order to achieve the needed selectivity, similar thermodynamic considerations require binding energy differences of CO2 over N2/O2 of at least 18 kJ mol⁻¹.3

The most striking difference between CO_2 and N_2 or O_2 is the magnitude of their molecular electric quadrupole moments. As linear molecules, the quadrupole tensor of all three can be characterized by their zz-component, the quadrupole moment Θ_{zz} , which is -3.19 au for CO₂, about 3 and 14 times larger than that of N₂ and O₂, respectively.^{6,7} The negative sign indicates that the two oxygen atoms located at either end of the molecule are negatively charged, while the central carbon atom is electron deficient; that is, the charge distribution is $(\delta -, 2\delta +, \delta -)$. While the much larger quadrupole moment of

Received: December 4, 2023 Revised: January 12, 2024 Accepted: January 17, 2024 Published: February 2, 2024





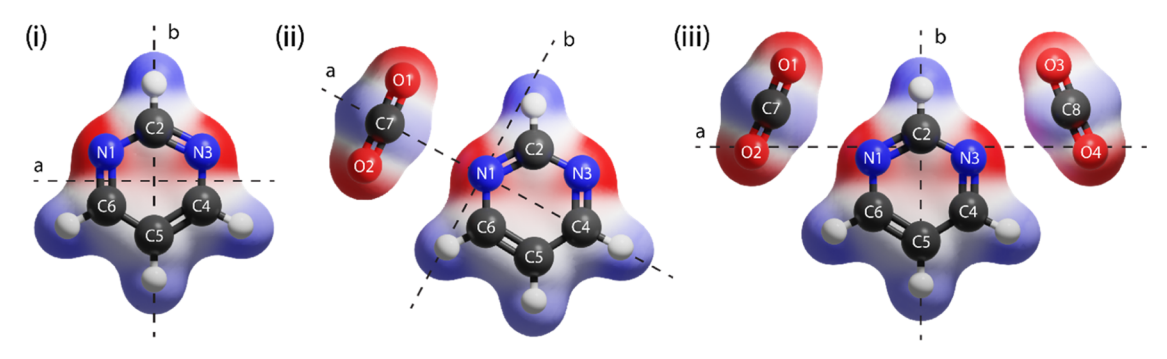


Figure 1. Structural diagrams of pyrimidine (i) and the $Pyr-(CO_2)_n$ complexes with n = 1,2, (ii), (iii) studied in this work. The a and b inertial axes are labeled, while the c axis, which lies perpendicular to the plane of the page, is omitted. Heavy atoms are labeled according to their position in the ring for the pyrimidine moieties and sequentially thereafter. Hydrogen atoms are labeled with the same numbering as the carbon atoms to which they are bound. Structures are calculated at the wB97X-D/6-311++G(3df,2p) level of theory.

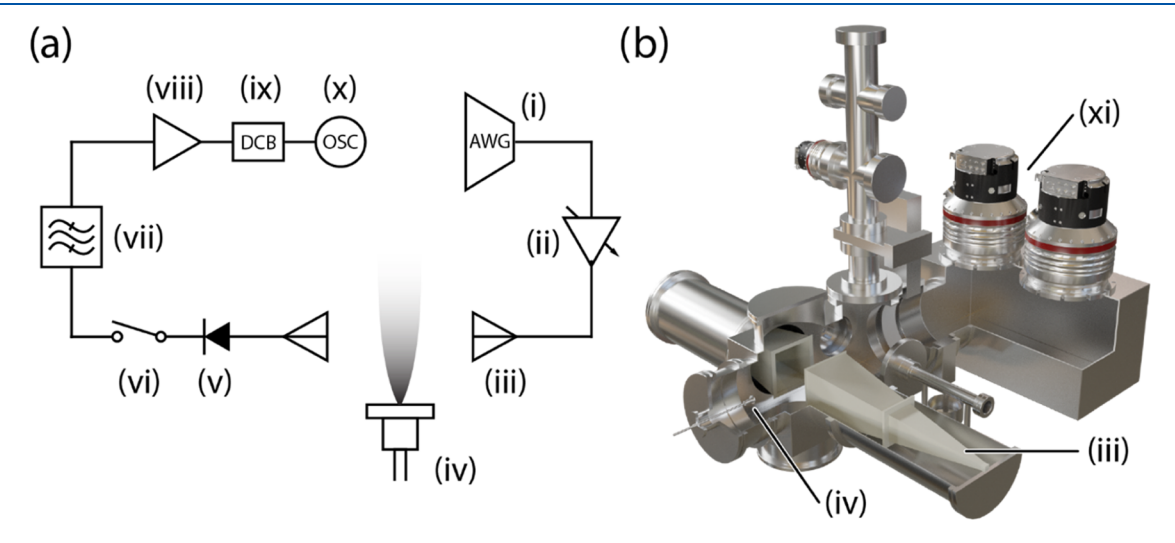


Figure 2. Depictions of the CP-FTMW instrument: (a) schematic of the microwave circuitry used to generate the excitation pulses and detect the resulting molecular free induction decay and (b) digital rendering of the vacuum chamber that houses both the microwave spectroscopy assembly and time-of-flight mass spectrometer. Component labels are referenced in-text.

 ${\rm CO_2}$ is widely recognized, it has not yet been utilized to great effect in ${\rm CO_2}$ capture.³

The present study takes a step back from the practical application of CO_2 capture to look in greater depth at a prototypical binding event between CO_2 and the molecule pyrimidine (Pyr), which has two localized quadrupolar binding pockets that are opposite in sign (i.e., +/-/+) to that of CO_2 , as shown in Figure 1. Our investigation is not without precedent. The recent microwave studies of Doran et al. characterized the pyridine- CO_2 complex, proving that CO_2 does bind to pyridine with its C atom centered on the single nitrogen heteroatom in a planar arrangement.⁸

Our focus on pyrimidine raises the question of whether a single molecule can profitably capture more than one CO_2 molecule in adjacent binding pockets in an analogous arrangement. We seek to determine then whether the first and second CO_2 molecules do in fact bind preferentially in these quadrupolar binding sites. As an alternative, one could imagine that the second CO_2 molecule might bind in a displaced stacked arrangement on the backside of the first CO_2 molecule, as it does in CO_2 dimer or in some other arrangement that derives maximum benefit from three-body interactions.

We use broadband microwave spectroscopy to record rotational spectra of Pyr- $(CO_2)_n$ with n = 1,2 in the 7.5-

17.5 GHz region. We also complement our experimental work with computational studies of the intermolecular potential energy surface, including an analysis of the intermolecular attractions using the effective fragment potential (EFP) method. $^{10-12}$ We compute binding energies and compare these with analogous calculations on Pyr-N $_2$ and Pyr-O $_2$ in order to assess the selectivity of the binding of CO $_2$ over the major components of air.

II. EXPERIMENTAL METHODS

Broadband microwave spectra of pyrimidine and its clusters with CO₂ were recorded using a chirped-pulse Fourier transform microwave (CP-FTMW) instrument described previously. The vacuum chamber shown in Figure 2b combines a broadband microwave spectrometer section capable of recording microwave spectra in the 2–18 GHz region with a time-of-flight mass spectrometer located immediately after the microwave horns. This latter capability is particularly useful when recording microwave spectra of reactive gas mixtures, where vacuum ultraviolet (VUV) single-photon ionization (118 nm) provides mass spectra to be correlated to the microwave spectra under different source conditions. This capability was not utilized in the present study.

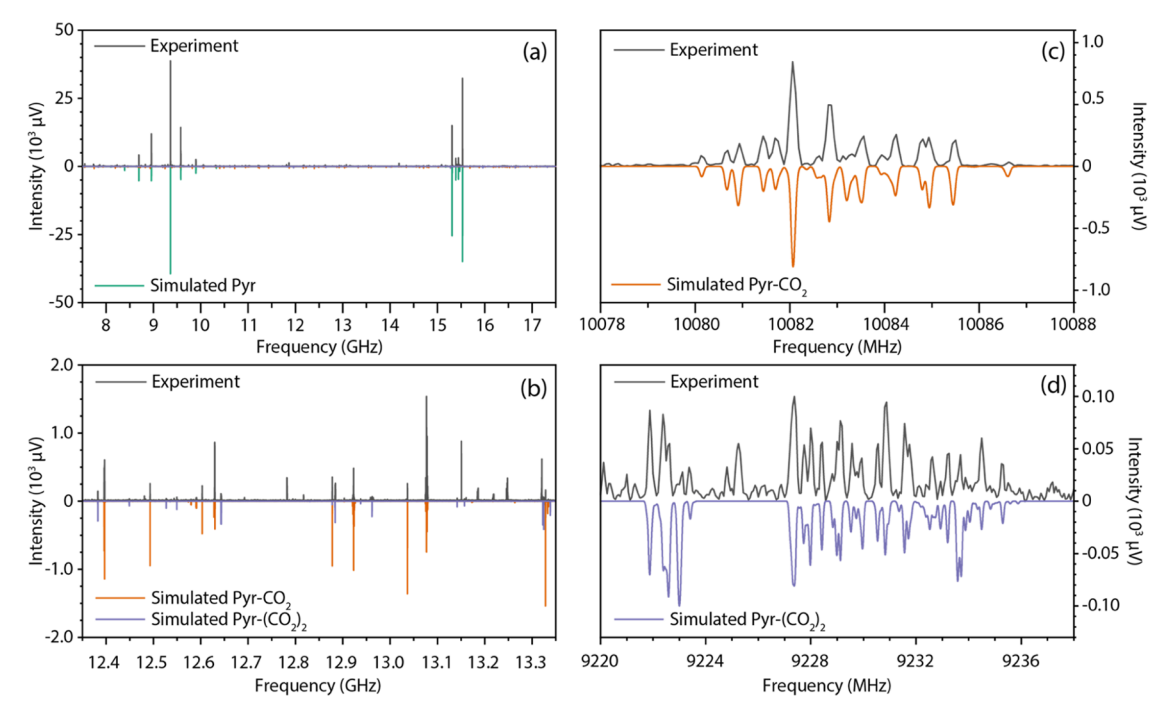


Figure 3. (a): Broadband microwave spectrum over the 7.5-17.5 GHz region of a mixture of pyrimidine at its room temperature vapor pressure expanded in a 0.75% CO₂ in the He mixture. Spectra simulated with a rotational temperature of 1.3 K using PGOPHER are shown inverted in each panel. The pyrimidine monomer is shown in green, fits to the Pyr-CO₂ complex are in orange, and those ascribed to Pyr-(CO₂)₂ are in purple. (b–d): 1.0 GHz, 10 and 18 MHz close-ups of the broadband spectrum in panel (a). The 14 N hyperfine splitting is partially resolved in the last two spectra.

Several improvements to the microwave spectrometer have been made since our earlier report. First, we have replaced the pumping system, which now consists of two 2150 L/s turbopumps (xi, Pfeiffer ATH 2303M) backed by a 1000 m³/h roots blower (Pfeiffer Okta 1000). The turbopumps are located behind the time-of-flight mass spectrometry (TOFMS) region. When operating a pulsed valve at 10 Hz, a maximum throughput of 1.69×10^{-3} bar·L/s is possible. Second, the microwave electronics have been upgraded to enable direct production and detection of microwave signals up to 20 GHz without mixing. A schematic diagram is shown in Figure 2a. A 65 GSa/s arbitrary waveform generator (AWG, (i), Keysight M8195A) produces a series of chirped pulses (typically 20 1 μ s long chirps separated by 20 μ s), each of which is a broadband chirp covering the 7.5-17.5 GHz region. The output from the AWG is switched on over a 400 μ s time window and amplified by a 200 W traveling-wave tube amplifier (TWTA, (ii), Amplifier Research 200T8G18A). The output of the TWTA is broadcast and received by a pair of horns ((iii), Steatite QWH-SL-2-18-S-HG-R) that cover the 2-18 GHz region. Unlike many other spectrometers, the broadcast and receiver horns are separated by only about 15 cm, sufficient for the unobstructed operation of a single pulsed valve (iv, Parker Series 9) between them.

The series of 20 microwave pulses interrogates the supersonic expansion that traverses the region between the horns. The ensemble of molecules and molecular clusters that absorb a given microwave pulse creates a macroscopic polarization that emits at the frequencies of the microwave transitions, creating a free induction decay (FID) in the time domain. This weak molecular emission signal is captured by the receiver horn. The excitation pulse has its power limited by a PIN diode (v) and is blocked from reaching the detection

electronics by a switch (vi) that is closed during each excitation pulse but opens within 650 ns for the molecular FID to pass through unobstructed. After filtering the noise from the switch with a 2-18 GHz band-pass filter (vii), a 50 dB low-noise amplifier (LNA, (viii), RF-Lambda RLNA06G18G45) operating in the 6-18 GHz region amplifies the signal, which is then passed through a DC block (ix) and fed directly into one of the channels of a digital oscilloscope ((x), Keysight Infiniium UXR 0204A) operating at 128 GSa/s. The scope has onboard memory sufficient to record the entire 400 μ s time window of the 20 molecular FIDs. Typical individual scans are recorded with the scope triggered at 10 Hz, the operating frequency of the pulsed valve, accumulating signal over 10,000 gas pulses (~17 min). The recorded FIDs are windowed using a Kaiser-Bessel function with an α parameter of 9.5, and then, a fast Fourier transform (FFT) of the FID produces a spectrum in frequency space.

For the study of Pyr- $(CO_2)_n$ clusters, we explored the best conditions for making the clusters. We achieved maximum cluster signal using a gas mixture consisting of 0.75% CO_2 in helium, which was bubbled through a sample of room temperature pyrimidine (R.T. vapor pressure of 17.9 Torr) placed just upstream of the pulsed valve. The stagnation pressure behind the pulsed valve was 2 bar, and the approximate flow rate of the CO_2/He mixture was 65 standard cm^3/min .

Since the scope averages an entire 400 μ s section of the gas pulse, we can carry out an FFT on each of the 20 FIDs in the 400 μ s trace. This is helpful for locating the best time window for detecting molecular clusters of a given size. Once this time window is established, deep averaging leads to the final time-domain trace and a MATLAB script is used to coadd the FIDs within the gas pulse. Phase stability was best realized by using

the leak-through from the chirp to align the individual FIDs in the set of 20 detected. As a result, no external clock signal from a stable frequency source is needed to maintain phase coherence over the time scales of these acquisitions. The typical fwhm line width of transitions measured using this spectrometer is approximately 150 kHz.

III. COMPUTATIONAL METHODS

With one exception, geometry optimizations of the complexes of interest, followed by harmonic vibrational frequency calculations, were carried out at the wB97X-D/6-311+ +G(3df,2p) level of theory as implemented in the GAMESS 2019 R1 suite of programs. Subsequently, to get interaction energies, energy decomposition analysis (EDA) calculations of the optimized geometries were performed at the CCSD(T)/6-311++G(3df,2p) level of theory, while EFP interaction energy calculations at the optimized geometries were conducted with the LIBEFP software. Geometries were conducted with the LIBEFP software. Software with the hybrid basis set 6-31G(d)/6-311++G(3df,2p) level of theory. Warnel of GAMESS on monomer geometries that were previously optimized at the wB97X-D/6-311++G(3df,2p) level of theory.

Since neither the CCSD(T) method nor MAKEFP calculations of open-shell molecules are implemented in GAMESS, we compared the binding of O_2 to that of N_2 and CO_2 and calculated the interaction energies of all of the dimers using the SAPT0 method. SAPT0/jun-cc-PVDZ interaction energies were computed at the optimized geometries of the dimers with the PSI4 quantum chemistry package.

In order to obtain final binding energies in Pyr-(CO₂)_{1,2}, corrections for basis set superposition error (BSSE)²² and zero-point energy (ZPE) were also made. The latter correction is especially important for molecular complexes since there are five additional intermolecular vibrational modes produced by complex formation, which add to the zero-point energy of the complex/cluster and hence reduce the net binding energy.

IV. RESULTS AND ANALYSIS

IV.I. Broadband Microwave Spectra. Figure 3a shows an overview spectrum (7.5-17.5 GHz) of 1% pyrimidine and 0.75% CO_2 in helium expansion. The signal from the pyrimidine monomer dominates the spectrum so that transitions from the CO_2 -containing clusters are barely visible when the monomer transitions are kept on the scale. These transitions are well-known from previous work²³ and include the nuclear hyperfine structure (also not visible in the overview scan) due to the presence of two I=1 nuclei from ¹⁴N.

Transitions due to a Pyr-CO₂ complex, with intensities at least 30 times smaller than the free pyrimidine, were identified using the optimized structure for the complex as a starting point for the fit, which was carried out in PGOPHER. ^{24,28} Simulated spectra were convolved with a 150 kHz fwhm Gaussian to match the experimental line width. Transitions due to the complex are shown at two amplifications of the frequency scale, with Figure 3b presenting a 1 GHz section and Figure 3c,d showing close-up views of the nuclear hyperfine structure. Transitions in the best-fit simulation of the Pyr-CO₂ spectrum are shown in orange. As Table 1 shows, a total of 313 transitions (across 105 distinct rotational transitions) were fit to an RMS error of 26.5 kHz, including the nuclear hyperfine structure. Intensities were fit best with a rotational temperature of 1–2 K. The calculated nuclear quadrupole terms were

Table 1. Best-Fit Rotational Parameters (Watson's A-Reduced Hamiltonian, I^r Representation) for the Pyr-CO₂ Complex Compared with Computed Predictions Based on the Optimized Structures at the wB97X-D/6-311+ +G(3df,2p) Level of Theory

parameter	experiment	wB97X-D
$A (MHz)^a$	4070.9891(14)	4114.1794
$B (MHz)^a$	859.41602(61)	860.14379
$C (MHz)^a$	710.02246(49)	711.41052
$\Delta_I (\mathrm{kHz})^b$	0.3122(30)	0.3007
$\Delta_{JK} (kHz)^b$	0.446(22)	0.490
$\Delta_K (\mathrm{kHz})^b$	0.47(17)	-0.29
$\delta_{J} (\mathrm{kHz})^{b}$	0.0562(13)	0.0552
$\delta_K (\mathrm{kHz})^b$	1.20(13)	1.01
$\chi_{\rm aa~(N1)}~({ m MHz})^c$	-4.551(13)	-4.921
$\chi_{\text{bb-cc (N1)}}$ (MHz) ^c	-1.833(27)	-2.149
$\chi_{aa (N3)} (MHz)^c$	-0.239(21)	-0.354
$\chi_{\mathrm{bb-cc}\;(\mathrm{N3})}\;(\mathrm{MHz})^c$	-6.394(27)	-7.021
N^d	313	
$\sigma (kHz)^e$	26.7	
$\Delta (\text{amu}\cdot \text{Å}^2)^f$	-0.41	0.00

^aRotational constants of the principal axes of inertia. ^bQuartic centrifugal distortion constants. ^cDiagonal components of the nuclear quadrupole interaction for each nitrogen atom. ^dNumber of assigned transitions used in the fit. ^eStandard error in fit transition frequencies. ^fInertial defect, given by $\Delta = I_c - I_a - I_b$ where I_x is the moment of inertia with respect to axis x.

different than those of pyrimidine monomer due to the rotation of inertial axes and shift in the center-of-mass in the complex. The assigned transitions are included in the Supporting Information. The rotational constants from the fit have an inertial defect of $-0.41~\text{amu-$\mathring{A}^2$}$, proving that the complex is planar. The small nonzero value for Δ is likely the result of the out-of-plane zero-point motion of the CO_2 molecules in the complex, leading to a small out-of-plane component to the vibrationally averaged structure. Complexation of a single CO_2 molecule causes a rotation of the principal inertial axes that produces intensity in both a- and b-type rotational transitions.

Table 1 also contains the best-fit values for the ¹⁴N hyperfine coupling constants, which show a significant shift compared to those of free pyrimidine due to both the rotation of the inertial axes in the complex as well as the subsequent breaking of the equivalence of the two ¹⁴N nuclei.

After identification of the pyrimidine monomer and Pyr-CO₂ transitions, there remained many transitions that grew in with the CO₂ concentration. The majority of these transitions could be fit to rotational parameters consistent with a structure for the Pyr-(CO₂)₂ cluster (shown in purple in Figure 3b,d), with the second CO₂ molecule taking up a position similar to the first one in the opposite quadrupolar binding pocket. The best-fit rotational parameters are listed in Table 2. Consistent with this structure, only b-type transitions are observed in the spectrum, indicating that the n=2 cluster has $C_{2\nu}$ symmetry. The fitted rotational constants once again reflect a planar structure with a near-zero inertial defect Δ (-0.41 amu-Å²). A total of 208 transitions (across 105 distinct rotational transitions) were fit to an RMS error of 29.8 kHz.

As an added assurance that both sets of transitions belonged to complexes involving pyrimidine, the fit ¹⁴N hyperfine coupling constants were recast from the inertial axis framework

Table 2. Best-Fit Rotational Parameters (Watson's A-Reduced Hamiltonian, I^r Representation) for the Pyr- $(CO_2)_2$ Cluster Compared with Computed Predictions of the Optimized Structure at the wB97X-D/6 311+ +G(3df,2p) Level of Theory

experiment	wB97X-D
1660.4513(11)	1645.1448
374.78338(41)	375.59893
305.84384(32)	305.78574
0.18224(88)	0.217
-2.6643(57)	-3.239
16.007(40)	19.130
0.05626(41)	0.06893
0.300(25)	0.405
-2.999(25)	-3.269
-3.414(24)	-3.816
208	
29.8	
-0.41	0.00
	1660.4513(11) 374.78338(41) 305.84384(32) 0.18224(88) -2.6643(57) 16.007(40) 0.05626(41) 0.300(25) -2.999(25) -3.414(24) 208 29.8

"Rotational constants of the principal axes of inertia. ^bQuartic centrifugal distortion constants. ^cDiagonal components of the nuclear quadrupole interaction for both equivalent nitrogen atoms. ^dNumber of assigned transitions used in the fit. ^eStandard error in fit transition frequencies. ^fInertial defect, given by $\Delta = I_c - I_a - I_b$ where I_x is the moment of inertia with respect to axis x.

(a, b, c) into the principle nuclear axis framework (x, y, z) using the QDIAG program²⁶ and were found to be a close match to those of free pyrimidine.²⁷ The details of this analysis are outlined in the Supporting Information.

V. DISCUSSION

V.I. Structural Analysis. Pyrimidine has two complementary quadrupolar binding pockets (+/-/+) for CO_2 (-/+/-) that also match reasonably well in spatial extent with the size of CO_2 . The two CH groups that constitute the ends of each of pyrimidine's two quadrupolar binding pockets have C(2)... C(4/6) separations of $R_{CC} = 2.26$ Å while the O···O separation in CO_2 is $R_{OO} = 2.31$ Å. By studying the properties of the complexes between pyrimidine and CO_2 , we gain insight into quadrupolar binding as a means for the capture and release of CO_2 . Furthermore, the two binding pockets, while distinct, are immediately adjacent to one another, raising the possibility that the energetics of binding a second CO_2 molecule might be influenced by the presence of a CO_2 molecule in the first binding site.

The rotational spectra of Pyr-CO₂ and Pyr-(CO₂)₂ prove that both CO₂ molecules bind to pyrimidine in the plane of the aromatic ring, with the center-of-mass of CO₂ residing near the lone pair of the nitrogen atom. This points clearly to an electrostatic binding through that interaction. In addition, the fact that the CO₂ molecules bind in the plane of pyrimidine, rather than perpendicular to it, is consistent with a distinct attraction of the oxygens of CO₂ to the CH groups ortho to the nitrogen. The calculated intermolecular N···C distances of Pyr-CO₂ and Pyr-(CO₂)₂ are 2.84 and 2.85 Å, respectively. Rotation of a CO₂ moiety in either complex to 90° out of the plane of the pyrimidine results in an approximately 0.14 Å elongation of this distance, as the O···H attractions are lost.

Finally, without ¹³C and/or ¹⁸O isotopic data, we do not have a firm experimental measure of the orientation of the CO₂ molecule in the plane of the complex. In pyridine-CO₂, Doran

et al. used data on isotopomers to show that the CO_2 molecule undergoes large amplitude in-plane bending. In pyrimidine, the two hydrogens that circumscribe the binding pocket are inequivalent, and this is calculated to produce an asymmetry to the binding pocket in Pyr-CO₂, with an O(1)··· H(2) distance of 3.30 Å and an O(2)–H(6) distance of 2.88 Å (Figure 1).

In Pyr- $(CO_2)_2$, the position and orientation of the two CO_2 molecules are the same by symmetry. They are also nearly identical to those in the Pyr- CO_2 complex, with calculated N··· C intermolecular distances in Pyr- $(CO_2)_2$ being only 0.01 Å longer than the N··· C distance in Pyr- CO_2 . This small increase is the only indication of a possible three-body interaction involving the two CO_2 molecules.

V.II. Contributions to the Interaction Energy. In order to understand the nature and magnitude of the binding between pyrimidine and CO_2 , we have carried out binding energy calculations for the n=1 and n=2 clusters and employed the EFP and SAPT0 methods to carry out an EDA that dissects the total interaction energy into well-known contributions to the intermolecular interaction due to electrostatics, polarization, dispersion, and exchange-repulsion. The top two lines of Table 3 list the calculated total interaction

Table 3. Total Interaction Energies ΔE (cm⁻¹; kJ mol⁻¹) of Pyr-X Complexes Calculated at the Indicated Levels of Theory^a

X	$CCSD(T)^{b}$	EFP/Hyb ^c	SAPT0 ^d
$CO_2(\parallel)$	-1496/-17.9	-1538/-18.4	-1656/-19.8
$2CO_2(\parallel)$	-2964/-35.5	-3016/-36.1	
$CO_2(\perp)$		-922/-11.0	-943/-11.3
$2CO_2(\parallel and \perp)$		-2408/-28.8	
$2CO_2(\perp)$		-1695/-20.3	
$N_2(\parallel)$	-410/-4.9	-400/-4.8	-293/-3.5
$2N_2()$	-830/-9.9	-768/-9.2	
$O_2(\parallel)$			-218/-2.6

^aThe CCSD(T) calculations do not include a BSSE correction. In their optimized structures, the X molecules are in their optimized positions in the plane of pyrimidine and are identified by the \parallel symbol in parentheses. Transitions state in which CO₂ is internally rotated about the C(7)···N or C(8)···N axis to an orientation in which the CO₂ axis is perpendicular to the plane of pyrimidine are labeled with \bot . ^b6-311++G(3df,2p) basis set; without the BSSE correction. ^cHybrid basis set: 6-31G* for electrostatics, 6-311++G(3df,2p) for all other terms. ^djun-cc-PVDZ basis set.

energies for Pyr-CO₂ and Pyr-(CO₂)₂ at the CCSD(T)/6-311++G(3df,2p) level of theory, with no BSSE correction, so that comparison with EFP and SAPT0 can be made directly. All of the structures of the complexes shown in Table 3 were optimized at the wB97X-D/6-311++G(3df,2p) level of theory and were confirmed to be minima in their corresponding potential energy surfaces by subsequent Hessian analysis. The agreement of the EFP and SAPT0 binding energies with each other and with the CCSD(T) calculations is excellent, giving confidence that the EDA will have good quantitative accuracy. The results for Pyr-CO₂ ($\Delta E = -1496 \text{ cm}^{-1} = -17.9 \text{ kJ} \text{ mol}^{-1}$) are also in good agreement with the previous best estimate of Vogiatzis et al. ($\Delta E = -1420 \text{ cm}^{-1} = -17.0 \text{ kJ} \text{ mol}^{-1}$). After the BSSE correction (200 cm⁻¹) and a harmonic zero-point energy correction carried out at the wB97X-D/6-311++G(3df2p) level of theory (153 cm⁻¹), we

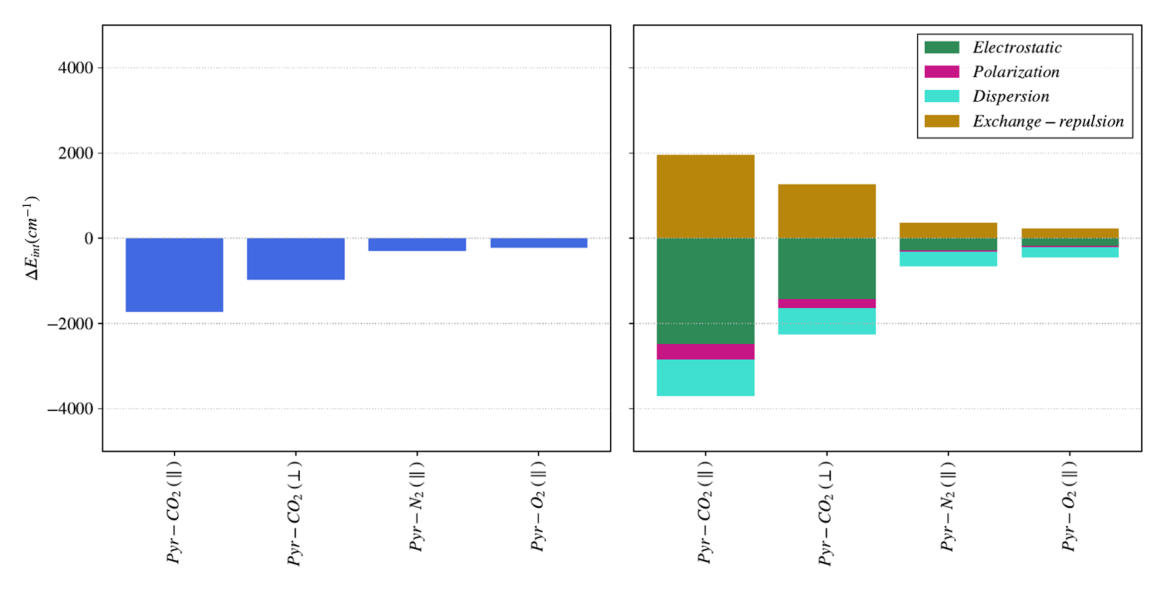


Figure 4. SAPT0 results for the total interaction energies (left) and the contributions to the pair interaction energy decomposition analysis of these interactions (right) for the Pyr-CO₂(\parallel), Pyr-CO₂(\perp), Pyr-N₂(\parallel), and Pyr-O₂(\parallel) complexes. Note that the energy scales are the same for both plots.

obtain a final calculated binding energy for Pyr-CO₂ of $\Delta E_0 = -1143 \text{ cm}^{-1} = -13.7 \text{ kJ mol}^{-1}$.

The analogous total interaction energy for the two CO_2 molecules in Pyr- $(CO_2)_2$ is almost precisely a factor of 2 greater than that for Pyr- CO_2 , indicating that three-body effects to the total binding energy are negligible when the two CO_2 molecules are in the two binding pockets.

To assess the magnitude of the interaction of the CO_2 oxygens with the CH groups at the two ends of the binding pocket, we first optimized transition states for the internal rotation of the CO_2 molecules about the N···C axis. The structures of the Pyr- $CO_2(\bot)$ and Pyr- $2CO_2(\parallel$ and $\bot)$ complexes in Table 3 were obtained by using saddle point calculations at the wB97X-D/6-311++G(3df,2p) level of theory. The structure of Pyr- $2CO_2(\bot)$, where both CO_2 molecules are perpendicular to the plane of pyrimidine, was obtained by manually rotating the CO_2 molecule that was in the plane of the Pyr- $(CO_2)_2(\parallel$ and $\bot)$ complex.

The calculated interaction energies ΔE based on the EDA for these perpendicular transition states are included in Table 3. Notably, both the EFP and SAPT0 interaction energies computed at the perpendicular transition state are about 40% smaller than the in-plane interaction energies, a surprisingly large effect that highlights the importance of the interaction of CO₂ with adjacent CH groups to the binding. This is borne out by the histogram displays of the SAPTO EDA analyses in Figure 4, which compare Pyr-CO₂(\parallel) and Pyr-CO₂(\perp). Numerical values for energy decomposition into electrostatics, polarization, dispersion, and exchange-repulsion are listed in Tables S1 and S2. The dominant contribution to the attractive interactions between pyrimidine and CO2 in its planar global minimum geometry is due to electrostatics (-2182 cm^{-1}) , with dispersion about one-third the size (-895 cm⁻¹). A similar distribution is observed in Pyr-CO₂(\perp), but reduced by about 40%, commensurate with the reduction in the total binding energy.

A further decomposition of the electrostatic terms in the EFP analysis into their contributions due to atom-centered charges, dipoles, and higher-order multipole terms is also included in Table S3. Figure 5 shows the atomic charges

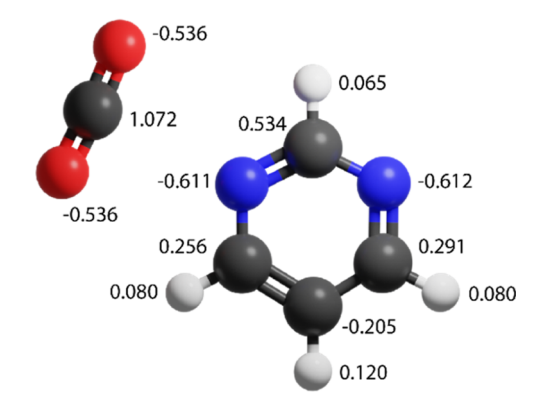


Figure 5. Optimized structure for the Pyr-CO2(\parallel) complex along with the EFP atomic charges.

extracted from the EFP analysis for the planar global minimum structure. Notably, the charge—charge interaction is 2-fold stronger in the Pyr-CO₂(\parallel) complex (1226 cm⁻¹) than in Pyr-CO₂(\perp) (594 cm⁻¹), confirming that, in addition to the N(δ -)····C(δ +) attraction between the pyrimidine nitrogen and CO₂ carbon, the interaction of the two oxygens of CO₂ with the two CH groups on either side of the N in pyrimidine is also primarily electrostatic in nature and a significant part of the binding. The 2-fold smaller interaction of CO₂ with pyrimidine in the perpendicular configuration is also likely affected by the repulsive interaction of the O atoms of CO₂ with the π -cloud. Nevertheless, referring to the binding between CO₂ and pyrimidine as locally quadrupolar in nature has validity.

Figure 6 extends the EFP EDA to the Pyr- $(CO_2)_2$ clusters with the two CO_2 molecules in parallel, one parallel/one perpendicular, and two perpendicular configurations. While the total interaction energies of the two CO_2 molecules are, to a good approximation, a simple sum of the single CO_2 interactions, there are small differences that indicate that the two CO_2 molecules are not completely independent of one another. For instance, the global minimum ($\|$, $\|$) configuration has a calculated total interaction energy that is about 50 cm $^{-1}$

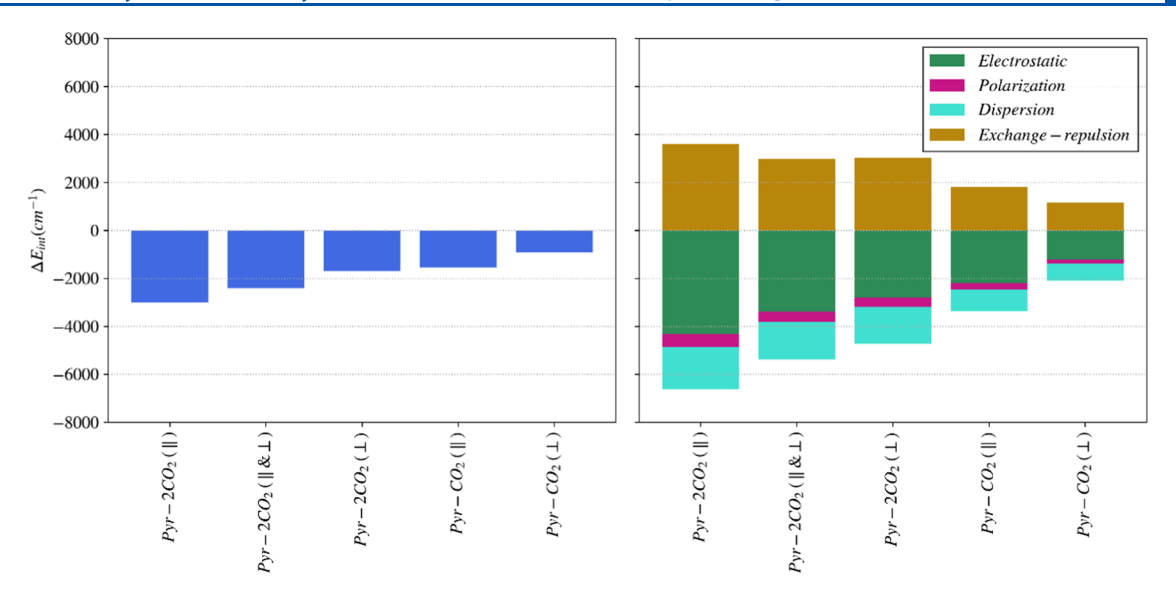


Figure 6. EFP results comparing the total binding energies (left) and EDA (right) for the (\parallel , \parallel), (\parallel , \perp), and (\perp , \perp) structures of Pyr-(CO₂)₂. The results for the Pyr-CO₂(\parallel) and (\perp) complexes are included for comparison. Note that the energy scales are the same on both plots.

Table 4. Thermochemical Calculations for Complex Formation in the Indicated Complexes

	interaction energy, ΔE^a		ΔZPE^{b}		ΔTC^c	ΔE (298 K)	ΔH (298 K)	ΔS (298 K)	ΔG (298 K)
complex	cm ⁻¹	kJ mol ⁻¹	cm ⁻¹	kJ mol⁻¹	kJ mol ⁻¹	kJ mol ⁻¹	kJ mol ⁻¹	J mol ⁻¹ K ⁻¹	kJ mol ⁻¹
Pyr- $CO_2()$	-1260	-15.1	155	1.9	4.6	-8.6	-11.1	-91.8	+16.2
$Pyr-(CO_2)_2(\parallel)$	-2492	-29.8	292	3.5	9.3	-17.0	-22.0	-179	+31.5
Pyr- $N_2(\parallel)$	-304	-3.6	111	1.3	5.1	+2.8	+0.3	-56.3	+17.1
$Pyr-(N_2)_2(\parallel)$	-615	-7.4	186	2.2	10.5	+5.3	+0.4	-103	+31.2
$Pyr-O_2(\parallel)$	-206	-2.5	79	0.9	5.4	+3.8	+1.4	-38.7	+12.9

^aInteraction energy (ΔE) calculated at the wB97X-D/6-311++G(3df,2p) level of theory, after correction for BSSE. ^bZero-point energy correction to the binding energy. ^cThermal contribution to ΔE (T) at T=298 K.

smaller than twice the Pyr-CO₂(\parallel) value, with a charge–charge attraction of 2431 cm⁻¹. An even larger reduction (~145 cm⁻¹) from twice the single \perp CO₂ binding is observed in the (\perp , \perp) second-order transition state. Once again, changes in the electrostatic charge–charge terms dominate the changes in the total binding energies at all CO₂ configurations.

Finally, Table 3 also includes total interaction energies for Pyr-N₂ and Pyr-O₂ for comparison with Pyr-CO₂. The results in Table 3 concentrate on competitive binding in pyrimidine's CO₂ binding pocket, recognizing that N₂ and O₂ may interact nearly as strongly with the aromatic π cloud as with the quadrupolar binding sites at the N atoms. The SAPTO calculations predict binding energies for Pyr-N₂ and Pyr-O₂ that are 6–8 times smaller than those in Pyr-CO₂. One would anticipate, on this basis, good selectivity for binding CO₂ over the major constituents of air. We are unaware of any experimental data on the Pyr-N₂ or Pyr-O₂ complexes.

V.III. Thermodynamic Assessment of Pyrimidine in the Context of CO_2 Capture and Release. Our spectroscopic studies of the Pyr- CO_2 complex were carried out following its formation in a supersonic expansion where the complex was in its vibrational zero-point level. As a result, the discussion thus far has focused attention on D_e and D_0 , which can be calculated quite accurately at the levels of theory used here.

However, in real-world applications, the capture of CO_2 by physisorption will likely occur at or near ambient conditions (T = 298 K). As Oschatz et al. have recently argued,³ in order for CO_2 capture to be efficient, we need $\Delta G/RT \le -4$, which

requires ΔG (298 K) ≤ -10 kJ mol⁻¹. However, there is a steep entropic penalty associated with forming the bound complex from two free molecules

$$Pyr(g) + CO_2(g) \leftrightharpoons Pyr \cdots CO_2(g)$$
 (1)

since the three translational and two rotational degrees of freedom of free CO_2 are lost in forming the bound complex. These five degrees of freedom become intermolecular (IM) vibrations of the complex. Oschatz et al. state that a typical entropic penalty for CO_2 physisorption is $T \cdot \Delta S$ (298 K) \approx -20 kJ mol⁻¹, putting a limit on the enthalpy of complex formation of $\Delta H \leq -30$ kJ mol⁻¹.

The calculated total binding energy for the binding of CO_2 to pyrimidine is $\Delta E_0 = -13.7 \text{ kJ mol}^{-1}$, which is just less than half the ΔH needed for efficient complex formation at room temperature. Nevertheless, in order to make this comparison directly, it is worth assessing the thermal contributions to ΔE , ΔH , ΔS , and ΔG in more detail since this could be useful in future experiments and modeling of CO_2 physisorption.

Since we are considering the case where the individual molecules and complex are all isolated and thus experience no interactions with their surroundings (see eq 1), we can use the thermodynamic quantities that are standard outputs of vibrational frequency calculations done in electronic structure packages, based on the optimized structures for pyrimidine, CO_2 , and $Pyr-CO_2$. Note that these results are based on a harmonic vibrational frequency analysis for all of the

vibrations, including the intermolecular vibrations, a point to which we will return later.

Table 4 presents the relevant thermodynamic quantities for Pyr-CO₂ and compares them to the corresponding quantities calculated at the same level of theory for Pyr-N₂ and Pyr-O₂; that is, for the complexes between pyrimidine and the main components of air. The table displays the total interaction energy of each complex, including the correction for BSSE, the correction for ZPE effects (Δ ZPE), and the thermal contribution to the internal energy change (Δ TC), leading to the expression for Δ E (298 K)

$$\Delta E (T = 298 \text{ K}) = \Delta E_0 + \Delta TC = \Delta E + \Delta ZPE + \Delta TC$$
(2)

In the ideal gas limit, ΔH and ΔE are related by the change in the number of gas-phase molecules during complex formation, with $\Delta n_g = -1$ for Pyr-CO₂ and $\Delta n_g = -2$ for Pyr-(CO₂)₂.

$$\Delta H (T) = \Delta E (T) + \Delta (P \cdot V) = \Delta E (T) + (\Delta n_g) RT$$
(3)

In the Supporting Information, we develop a simple model for the thermodynamics of complex formation that provides some insight as to the major factors contributing to the thermal contributions to ΔE . The model focuses attention on the three major changes that accompany the formation of a complex between CO_2 and a binding partner: (i) the loss of three translational degrees of freedom of the CO_2 molecule, (ii) the loss of the two rotational degrees of freedom of CO_2 , and (iii) the formation of five new intermolecular vibrations, all of which are low-frequency vibrations in which $\omega_\mathrm{e} \ll kT$, where $kT=208~\mathrm{cm}^{-1}$ at $T=298.15~\mathrm{K}$. We also assume that the intramolecular vibrational frequencies of pyrimidine and CO_2 are not changed significantly by complex formation.

The five lost translational and rotational degrees of freedom each contribute -1/2RT to ΔE (298 K), while each of the five new intermolecular vibrations, with their low frequencies, contribute up to +RT. Thus, for complex formation

$$\Delta H (T) \approx \Delta E_0 + \frac{1}{2} (\text{\#IM vibrations}) \cdot RT - RT$$

$$= \Delta E_0 + \frac{3}{2} RT \tag{4}$$

For Pyr-CO₂, this simple estimate yields ΔH (298 K) \approx -9.6 kJ mol⁻¹, compared to -11.2 kJ mol⁻¹ from the full harmonic calculation in Table 4.

The entropy change associated with complex formation contains many competing terms. The loss of three translations and two rotations from CO₂ contributes two large negative terms to ΔS . In the limit that $m_X\gg m_{\rm CO2}$, $\Delta S_{\rm rot}\approx -S_{\rm rot}({\rm CO}_2)$ and $\Delta S_{\rm trans}\approx -S_{\rm trans}({\rm CO}_2)$. This rudimentary model predicts values for any X-CO₂ complex of $\Delta S_{\rm trans}=-18.7R$ and $\Delta S_{\rm rot}=-7.3R$. When the partition functions for pyrimidine, CO₂, and Pyr-CO₂ are all included, we obtain $\Delta S_{\rm trans}=-18.1R$ and $\Delta S_{\rm rot}=-5.3R$. The larger correction to $\Delta S_{\rm rot}$ indicates that changes in rotational constants of Pyr relative to Pyr-CO₂ are not entirely negligible and partly compensate for the large negative contribution from the loss of CO₂ rotation.

By contrast, the formation of five low-frequency intermolecular modes in the Pyr-CO $_2$ complex produces a large positive contribution to ΔS .

$$\Delta S_{v} (298 \text{ K}) \approx S_{v,\text{IM}} = \left\{ 5 + \sum_{i=1}^{5} \left[\ln \left(\frac{208}{\omega_{e,i}} \right) \right] \right\} \cdot R$$
 (5)

Inserting the five intermolecular vibrational frequencies for Pyr-CO₂, we see that $\Delta S_{\rm v} = +11.5R$. Combining the translational, rotational, and vibrational terms, $\Delta S_{\rm tot} = -12.2R = -101~{\rm J~mol}^{-1}~{\rm K}^{-1}$, compared to $-91.8~{\rm kJ~mol}^{-1}$ for the full harmonic calculation.

Finally, combining ΔH and ΔS , we have a final estimate for ΔG (Pyr-CO₂, 298 K) \approx +20.5 kJ mol⁻¹, compared to +16.2 kJ mol⁻¹ for the full harmonic calculation (Table 4). We see that the model accounts for the main factors contributing to ΔG (T). Notably, whether we use the model calculation or the full harmonic calculation from Table 4, $\Delta G/RT$ is positive and large enough that the equilibrium in eq 1 is pushed far to the left toward unbound reactants at T=298 K.

While this estimate makes it clear that Pyr-CO₂ has an interaction energy too small for optimal binding for CO2 sequestration, the calculation of ΔG (298 K) from Table 4, which uses the harmonic oscillator/rigid-rotor treatment available in standard electronic structure packages, is not anticipated to be quantitatively accurate when applied to weakly bound complexes.^{30,31} First, even in the limit that all vibrations are adequately treated as harmonic oscillators, the vibrational contribution to the entropy is extraordinarily sensitive to the vibrational frequencies of the intermolecular vibrations, which are difficult to calculate with quantitative accuracy. Second, the harmonic approximation necessarily assumes that all vibrations have an infinite number of bound levels that can store energy and entropy as the temperature increases. However, the intermolecular vibrations are far from harmonic, as the actual intermolecular potential energy surface supports a finite number of bound levels in which CO₂ moves around the surface of the pyrimidine molecule with increasing amplitude. These deficiencies of the standard analysis are more obvious in Pyr-O2 and Pyr-N2, where even the thermal corrections to ΔE in the harmonic limit are bigger than the binding energy itself, leading to ΔE (298 K) values that are calculated to be positive at 298 K. In such weakly bound complexes, the calculated values for ΔS are also likely to have large errors, rendering any comparisons of ΔG for N_2 , O_2 , and CO₂ to be of little quantitative value in assessing selectivity.

In order to carry out a quantitatively accurate free energy calculation, it seems likely that ab initio molecular dynamics calculations will be needed to map out the path integrals directly, including quantum effects, as Bishop and Roy recently described.³⁰ Such a calculation is outside the scope of this work but is likely to be important to predict CO₂ binding propensities of greater accuracy.

VI. CONCLUSIONS

In this work, we have obtained broadband microwave spectra of the gas-phase complexes of Pyr-CO₂ and Pyr-(CO₂)₂ and determined that the first and second CO₂ molecules take up equivalent binding sites, with the C atom of CO₂ bound to the N lone pair of pyrimidine and the two oxygens in-plane where they can interact with the two CH hydrogens ortho to the N atoms. The calculated barrier to internal rotation of CO₂ about the N···C axis is a significant fraction of the total binding energy, indicating that CO₂ is sensitive to the (+/-/+) pyrimidine binding pocket that is complementary to its (δ -/ 2δ +/ δ -) quadrupole. By comparison of the calculated

interaction energies and the EFP analysis of the binding, it is clear that both the well-placed local electrostatic configuration and better size match of CO_2 with the pyrimidine pocket play a role in increasing the total binding energy relative to N_2 and O_2 , the major components of air. While the total binding energy of each CO_2 to pyrimidine is insufficient on its own to be a strong CO_2 sequestration agent, the present study illustrates the role that quadrupolar binding sites can play in trapping CO_2 via physisorption.

Such quadrupolar binding sites may play a role in carbon capture processes that do not rely purely on gas-phase binding. Recent work on CO₂ uptake and transport in clay interlayers would benefit from the infusion of binding partners that would increase the rate and selectivity of uptake.³² Pyrimidine is one of the partners being considered, as it is ubiquitous in nature, has a planar structure compatible with the sheetlike clay interlayer, and has the potential for enhanced binding to CO₂ under conditions of nanoconfinement in the high ionic strength aqueous interlayer.

ASSOCIATED CONTENT

Supporting Information

The Supporting Information is available free of charge at https://pubs.acs.org/doi/10.1021/acs.jpca.3c07930.

Detailed description of the model for the thermodynamics of complex formation; numerical values of the energy decomposition analysis; full assigned line lists for Pyr-CO₂ and Pyr-(CO₂)₂; rationale for the choice of the I^r representation for the complexes, and details of the recasting of the ¹⁴N hyperfine constants into the principle nuclear axis system (PDF)

AUTHOR INFORMATION

Corresponding Authors

Lyudmila V. Slipchenko – Department of Chemistry, Purdue University, West Lafayette, Indiana 47907-1393, United States; orcid.org/0000-0002-0445-2990;

Email: lslipchenko@gmail.com

Timothy S. Zwier — Gas Phase Chemical Physics, Sandia National Laboratories, Livermore, California 94550, United States; © orcid.org/0000-0002-4468-5748;

Email: tszwier@sandia.gov

Authors

Blair A. Welsh – Gas Phase Chemical Physics, Sandia National Laboratories, Livermore, California 94550, United States

Andres S. Urbina — Department of Chemistry, Purdue University, West Lafayette, Indiana 47907-1393, United States; oocid.org/0000-0001-6482-4736

Tuan A. Ho — Geochemistry Department, Sandia National Laboratories, Albuquerque, New Mexico 87185, United States; Occid.org/0000-0002-8129-1027

Susan L. Rempe — Center for Integrated Nanotechnologies, Sandia National Laboratories, Albuquerque, New Mexico 87185, United States; © orcid.org/0000-0003-1623-2108

Complete contact information is available at: https://pubs.acs.org/10.1021/acs.jpca.3c07930

Notes

The authors declare no competing financial interest.

ACKNOWLEDGMENTS

B.A.W., T.A.H., S.L.R., and T.S.Z. were supported in this work by the Laboratory Directed Research and Development program at Sandia National Laboratories, a multimission laboratory managed and operated by National Technology and Engineering Solutions of Sandia LLC, a wholly-owned subsidiary of Honeywell International Inc. for the U.S. Department of Energy's National Nuclear Security Administration under contract DE-NA0003525. The views expressed in the article do not necessarily represent the views of the U.S. DOE or the United States Government. L.V.S. and A.S.U. gratefully acknowledge support from the National Science Foundation (grant CHE-2102639).

REFERENCES

- (1) Kerry, J.; McCarthy, G. The Long-Term Strategy of the United States: Pathways to Net-Zero Greenhouse Gas Emissions by 2050; United States Department of State: Washington DC, 2021.
- (2) Custelcean, R. Direct Air Capture of CO2 Using Solvents. *Annu. Rev. Chem. Biomol. Eng.* **2022**, *13*, 217–234.
- (3) Oschatz, M.; Antonietti, M. A search for selectivity to enable CO2 capture with porous adsorbents. *Energy Environ. Sci.* **2018**, *11* (1), 57–70.
- (4) McQueen, N.; Gomes, K. V.; McCormick, C.; Blumanthal, K.; Pisciotta, M.; Wilcox, J. A review of direct air capture (DAC): scaling up commercial technologies and innovating for the future. *Prog. Energy* **2021**, *3* (3), No. 032001.
- (5) Mannisto, J. K.; Pavlovic, L.; Tiainen, T.; Nieger, M.; Sahari, A.; Hopmann, K. H.; Repo, T. Mechanistic insights into carbamate formation from CO2 and amines: the role of guanidine-CO2 adducts. *Catal. Sci. Technol.* **2021**, *11* (20), 6877–6886.
- (6) Junquera-Hernández, J.; Sanchez-Marin, J.; Maynau, D. Molecular electric quadrupole moments calculated with matrix dressed SDCI. *Chem. Phys. Lett.* **2002**, 359 (3–4), 343–348.
- (7) Lawson, D. B.; Harrison, J. F. Distance dependence and spatial distribution of the molecular quadrupole moments of H-2, N-2, O-2, and F-2. *J. Phys. Chem. A* **1997**, *101* (26), 4781–4792.
- (8) Doran, J. L.; Hon, B.; Leopold, K. R. Rotational spectrum and structure of the pyridine-CO2 van der Waals complex. *J. Mol. Struct.* **2012**, *1019*, 191–195.
- (9) Yu, K.; Schmidt, J. R. Many-body effects are essential in a physically motivated CO2 force field. *J. Chem. Phys.* **2012**, *136* (3), No. 034503.
- (10) Flick, J. C.; Kosenkov, D.; Hohenstein, E. G.; Sherrill, C. D.; Slipchenko, L. V. Accurate Prediction of Noncovalent Interaction Energies with the Effective Fragment Potential Method: Comparison of Energy Components to Symmetry-Adapted Perturbation Theory for the S22 Test Set. J. Chem. Theory Comput. 2012, 8 (8), 2835—2843
- (11) Ghosh, D.; Kosenkov, D.; Vanovschi, V.; Williams, C. F.; Herbert, J. M.; Gordon, M. S.; Schmidt, M. W.; Slipchenko, L. V.; Krylov, A. I. Noncovalent Interactions in Extended Systems Described by the Effective Fragment Potential Method: Theory and Application to Nucleobase Oligomers. *J. Phys. Chem. A* **2010**, *114* (48), 12739–12754.
- (12) Gordon, M. S.; Smith, Q. A.; Xu, P.; Slipchenko, L. V. Accurate First Principles Model Potentials for Intermolecular Interactions. *Annu. Rev. Phys. Chem.* **2013**, *64*, 553–578.
- (13) Fritz, S. M.; Hays, B. M.; Hernandez-Castillo, A. O.; Abeysekera, C.; Zwier, T. S. Multiplexed characterization of complex gas-phase mixtures combining chirped-pulse Fourier transform microwave spectroscopy and VUV photoionization time-of-flight mass spectrometry. *Rev. Sci. Instrum.* **2018**, 89 (9), No. 093101.
- (14) Schmidt, M. W.; Baldridge, K. K.; Boatz, J. A.; Elbert, S. T.; Gordon, M. S.; Jensen, J. H.; Koseki, S.; Matsunaga, N.; Nguyen, K. A.; Su, S. J.; et al. General Atomic and Molecular Electronic-Structure System. *J. Comput. Chem.* **1993**, *14* (11), 1347–1363.

- (15) Su, P. F.; Li, H. Energy decomposition analysis of covalent bonds and intermolecular interactions. *J. Chem. Phys.* **2009**, *131* (1), No. 014102.
- (16) Kaliman, I. A.; Slipchenko, L. V. LIBEFP: A new parallel implementation of the effective fragment potential method as a portable software library. *J. Comput. Chem.* **2013**, 34 (26), 2284–2292.
- (17) Kaliman, I. A.; Slipchenko, L. V. Hybrid MPI/OpenMP Parallelization of the Effective Fragment Potential Method in the libefp Software Library. *J. Comput. Chem.* **2015**, *36* (2), 129–135.
- (18) Hands, M. D.; Slipchenko, L. V. Intermolecular Interactions in Complex Liquids: Effective Fragment Potential Investigation of Water-tert-Butanol Mixtures. *J. Phys. Chem. B* **2012**, *116* (9), 2775–2786.
- (19) Rankin, B. M.; Hands, M. D.; Wilcox, D. S.; Fega, K. R.; Slipchenko, L. V.; Ben-Amotz, D. Interactions between halide anions and a molecular hydrophobic interface. *Faraday Discuss.* **2013**, *160*, 255–270.
- (20) Parker, T. M.; Burns, L. A.; Parrish, R. M.; Ryno, A. G.; Sherrill, C. D. Levels of symmetry adapted perturbation theory (SAPT). I. Efficiency and performance for interaction energies. *J. Chem. Phys.* **2014**, *140* (9), No. 094106.
- (21) Turney, J. M.; Simmonett, A. C.; Parrish, R. M.; Hohenstein, E. G.; Evangelista, F. A.; Fermann, J. T.; Mintz, B. J.; Burns, L. A.; Wilke, J. J.; Abrams, M. L.; et al. PSI4: an open-source ab initio electronic structure program. WIREs Comput. Mol. Sci. 2012, 2 (4), 556–565.
- (22) Gray, M.; Bowling, P. E.; Herbert, J. M. Systematic Evaluation of Counterpoise Correction in Density Functional Theory. *J. Chem. Theory Comput.* **2022**, *18* (11), 6742–6756.
- (23) Caminati, W.; Damiani, D. Easy Assignment of Rotational Spectra of Slightly Abundant Isotopic-Species in Natural Abundance: C-13 And N-15 Isotopic-Species of Pyrimidine. *Chem. Phys. Lett.* **1991**, *179* (5–6), 460–462.
- (24) Western, C. M.; Billinghurst, B. E. Automatic assignment and fitting of spectra with PGOPHER. *Phys. Chem. Chem. Phys.* **2017**, 19 (16), 10222–10226.
- (25) Western, C. M.; Billinghurst, B. E. Automatic and semi-automatic assignment and fitting of spectra with PGOPHER. *Phys. Chem. Chem. Phys.* **2019**, *21* (26), 13986–13999.
- (26) PROSPE-Programs for Rotational Spectroscopy, 2000. http://info.ifpan.edu.pl/~kisiel/prospe.htmhttp://info.ifpan.edu.pl/~kisiel/prospe.htm. (accessed January 8, 2024).
- (27) Kisiel, Z.; Pszczolkowski, L.; López, J. C.; Alonso, J. L.; Maris, A.; Caminati, W. Investigation of the rotational spectrum of pyrimidine from 3 to 337 GHz:: Molecular structure, nuclear quadrupole coupling, and vibrational satellites. *J. Mol. Spectrosc.* 1999, 195 (2), 332–339.
- (28) Blackman, G. L.; Brown, R. D.; Burden, F. R. The microwave spectrum, dipole moment, and nuclear quadrupole coupling constants of pyrimidine. *J. Mol. Spectrosc.* **1970**, 35 (3), 444–454.
- (29) Vogiatzis, K. D.; Mavrandonakis, A.; Klopper, W.; Froudakis, G. E. Ab initio Study of the Interactions between CO2 and N-Containing Organic Heterocycles. *ChemPhysChem* **2009**, *10* (2), 374–383.
- (30) Bishop, K. P.; Roy, P. N. Quantum mechanical free energy profiles with post-quantization restraints: Binding free energy of the water dimer over a broad range of temperatures. *J. Chem. Phys.* **2018**, 148 (10), No. 102303.
- (31) Hansen, A. S.; Maroun, Z.; Mackeprang, K.; Frandsen, B. N.; Kjaergaard, H. G. Accurate thermodynamic properties of gas phase hydrogen bonded complexes. *Phys. Chem. Chem. Phys.* **2016**, *18* (34), 23831–23839.
- (32) Ho, T. A.; Wang, Y. F.; Rempe, S. B.; Dasgupta, N.; Johnston, C. T.; Xu, G. P.; Zwier, T. S.; Mills, M. Control of the Structural Charge Distribution and Hydration State upon Intercalation of CO2 into Expansive Clay Interlayers. *J. Phys. Chem. Lett.* **2023**, *14* (11), 2901–2909.